Chapter 7

Friction and Wear in Automotive Journal Bearings Operating in Today's Severe Conditions

David E. Sander, Hannes Allmaier and
Hans-Herwig Priebsch

Additional information is available at the end of the chapter

http://dx.doi.org/Chapter DOI: 10.5772/64247

Abstract

A current trend in the transport sector seeks to increase the vehicle efficiency and to cut fuel consumption which leads to new technologies and advancements in modern and future combustion engines. Some of these technical progresses lead to highly stressed engine parts and new challenges arise, particularly for journal bearings. The increasing thermal and mechanical load caused by downsized and turbocharged engines, friction reduction by employing low-viscosity lubricants and other emission reduction measures—for utilizing stop-start systems—put additional stress on the crankshaft journal bearings. This contribution focuses on highly stressed journal bearings which operate in the boundary, mixed and hydrodynamic lubrication regime. Therefore, measurements on a journal bearing test-rig are performed which allow an extensive verification of the numerical investigation. For the numerical analysis of friction and wear, a mixed elasto-hydrodynamic simulation approach is developed, which considers the elastic deformation of the contacting components, the complex rheological behaviour of the lubricant and metal-metal contact if the lubricant is unable to separate the contacting surfaces. Both the rheological data and the surface roughness parameters are obtained from measurements. The current challenges are studied in four application-oriented examples and the influencing parameters on a reliable friction and wear prediction are explored.

Keywords: simulation, hydrodynamic bearing, plain bearing, mixed friction, elasto-hydrodynamic lubrication, non-Newtonian lubricant, conformal contact, stop-start

1. Introduction and outline

A plain journal bearing is a seemingly simple machine element where a hardened shaft typically rotates in a softer bearing shell. The two contacting surfaces are generally separated by a lubricant. In most technical applications, such as turbines or combustion engines, journal bearings are designed for a long life time. Hence, journal bearings mainly operate in pure hydrodynamic lubrication regime. However, especially in the automotive industry, a trend has evolved to cut fuel consumption and emissions derived from emission restrictions by legislation and customer satisfaction. A cost-effective potential to improve the efficiency is attributed to the reduction of friction in lubricated contacts. The friction coefficient finds its minimum in the transition between pure hydrodynamic lubrication and mixed lubrication regime, where already some metal-metal contact between the shaft and bearing shell occurs. Therefore, it is beneficial to operate journal bearings in this transition, but unfortunately wear occurs as metal-metal contact establishes and durability problems may follow. To design more efficient journal bearings, a detailed simulation approach is required which is suited to describe the complex behaviour of mixed elasto-hydrodynamic lubrication and is validated for a wide range of operating conditions.

In addition, beyond the consequences of friction reduction many new modes of engine operation stress the bearings. Therefore, this chapter begins with a general overview of the current challenges for journal bearings, especially in combustion engine application.

Subsequently, the requirements for the simulation model are elaborated from these challenges at the beginning of the next section. In the same section, the basic equations for the mixed elasto-hydrodynamic journal bearing simulation are presented. Additionally, the simplified layout of the journal bearing test-rig and the simulation model is described which is used for the study on journal bearing friction and wear.

The subsequent result section consists of different application examples and provides an overview of the current research by the authors. The first example analyses friction of dynamically loaded journal bearings under extreme loading conditions which lead to fluid film pressures above 2000 bar and to high shear rates. The complex properties of the lubricant are central to these results. The second example concentrates on the running-in wear of journal bearings until a steady state of operation is achieved. The third example focuses on severe metal-metal contact and on friction in mixed lubrication regime. Therefore, a static load is applied to the journal bearing and Stribeck curves are calculated. Finally, a transient start-stop simulation is performed in the final example.

This chapter concludes with a comprehensive summary of the studied results and presents a brief outlook on future research topics.

2. Current challenges for journal bearings in combustion engines

In today's automotive engines, journal bearings operate under severe conditions. Here, these conditions will be discussed in more detail as they are the prime subject for the presented study and also for future research. A more comprehensive review can be found in [1].

http://dx.doi.org/Chapter DOI: 10.5772/64247

2.1. Turbocharged engines with high power density

Modern downsized combustion engines with turbocharger(s) achieve a high power output from small volume displacements and allow an efficiency improvement with lower emissions. At the same time, the high power density increases the thermal and mechanical load on the engine components. Additionally, the light-weight design of the engine further improves the vehicle performance. Hence, the engine and its component dimensions become smaller too. This implies even higher stresses on the components and the lubricated contacts. For instance, the big-end bearing of the connection rod has to resist specific loads above 100 MPa and a further increase is expected for future engines [2]. As a consequence, the minimum lubrication gap in the journal bearing decreases below 1 μm and metal-metal contact may occur at these operating conditions. Furthermore, the elastic deformations of the bearing shell and its surrounding parts have a major influence on bearing behaviour.

2.2. Stop-start system

One of the most widely used mechanisms to improve fuel economy, especially for urban driving, is the application of stop-start systems [3, 4]. By turning off the engine instead of operating it at idle (e.g. when waiting at crossings) significant fuel savings can be obtained [4, 5]. More recently, this procedure was extended to switching off the engine also during driving at very low loads which is commonly called engine coasting.

Stop-start systems have quickly become widely available, but despite their apparent simplicity the repeated stopping and starting of the engine present a big challenge for bearing manufacturers. When the engine is started the bearing has to overcome the boundary and mixed lubrication regime before a hydrodynamic film has formed, which completely separates the two contacting surfaces [6]. Thus, with the increasing number of stop-start cycles bearing wear will escalate.

2.3. Cylinder de-activation

Another fuel economy improvement is achieved through a cylinder de-activation technology (CDT) as a result of reduced air pumping losses. Further benefits are achieved due to an increased exhaust temperature under partial loading which yields an improved after-treatment efficiency for diesel engines. This will further help the three-way catalyst technology [7]. However, CDT affects the dynamic behaviour of the shaft and topics such as shaft bending and journal misalignment that are relevant for bearing design and bearing layout. The ability of the bearing shell to adapt its surface geometry and further to fit the deformed or misaligned shaft can become essential. Also, the friction power losses need to be investigated to show the overall efficiency benefits. A better understanding for the necessary redesign of the power train with CDT is the target in recent bearing simulation [8–10].

2.4. Ultralow-viscosity lubricants

The usage of low-viscosity lubricants in the automotive sector is certainly not new. However, the increasingly strict legislation forces the automotive industry to further increase engine

efficiency. Here, the usage of a lower viscosity lubricant is considered to be a very economic measure to reach this goal [11]. However, the current trend goes to lubricants with a drastically reduced viscosity and new standards had to be defined accordingly [12]. With the new SAE standards 16, 12, 8 and even lower classes being targeted, pure hydrodynamic lubrication conditions will increasingly decline and be replaced by mixed lubrication near the minimum friction coefficient [13].

2.5. Complex rheological properties of modern lubricants

It is well known that modern multi-grade lubricants show a non-Newtonian behaviour. At high shear rates, which typically occur in automotive journal bearings, the viscosity significantly drops below the viscosity at low shear rate. To assess this shear thinning behaviour, a viscosity at high temperature and high shear rate (HTHS-viscosity) is standardized. It is shown that the HTHS-viscosity directly affects the mechanical efficiency of the engine in fleet tests [14, 15], which demonstrates the necessity to realistically consider the non-Newtonian behaviour of the lubricant in the simulation. There exists a further lubricant property counteracting the non-Newtonian behaviour in journal bearings, which increases the lubricant viscosity locally under load. This lubricant property is called the piezo-viscous effect and it is present in both mono and multi-grade lubricants [16].

Currently, the required lubricant data are not stated in the lubricant datasheets as such measurements are not part of common standards. Therefore, such rheological data are only sparse. The interdependency of the piezo-viscous effect and the non-Newtonian behaviour makes it difficult not only to measure them, but also to include these properties accurately in simulation. Currently, commonly used approaches use, for example, the Barus equation and the Cross equation to consider these effects in a simulation independently from each other and independent of the lubricant temperature (e.g., [17]). While these are useful approximations of the reality and considerably increase the quality of the results, the true lubricant behaviour is still considerably more complex [18–20].

2.6. New classes of surface textures and coatings

To increase the durability and to reduce the friction loss in journal bearings, new techniques have grown in popularity in the process of manufacturing journal bearings. While still two- and three-layer journal bearings dominate the automotive industry, new development trends bring refined surface structuring techniques, such as polymer coatings and diamond-like carbon (DLC) coatings.

Surface texturing, which is the intentional modification of the journal bearing surface with regular patterns (dimples, microgrooves), has the potential to increase the load-carrying capacity [21]. Such surface texturing methods themselves are not new and are, for example, widely used in other parts of the internal combustion engine, namely, in honing of the cylinder liners. For journal bearings it is experimentally shown that surface textures can affect their tribological properties [22, 23] as well as the damping properties and the compatibility of the journal bearing with contaminants [24, 25]. The theoretical understanding of the underlying

http://dx.doi.org/Chapter DOI: 10.5772/64247

effects of surface textures is currently limited [26]. So far it is commonly accepted that cavitation plays a crucial part for this effect [27–29] as well as that surface textures have an influence on local micro-hydrodynamics [26].

Polymer coatings are increasingly available on the market and can offer better durability in start-stop conditions [30, 31]. As these coatings are non-metallic materials, their behaviour in terms of wear and plastic deformation is distinctly different to metallic materials. These coatings require new approaches to describe their behaviour realistically in the simulation [32, 33]. DLC coatings are already widely used in engines today, like for piston pins or cam tappets, which are highly loaded contacts and dominantly operate in mixed lubrication. Crankshaft journal bearings dominantly operate in hydrodynamic lubrication regime and an ability to adapt the bearing surface is often required which makes DLC coatings apparently inappropriate. Nonetheless, it was recently shown that DLC have a potential for friction reduction for the journal bearings of the crank train [34].

3. Journal bearing simulation

Before the basic equations for the elasto-hydrodynamic journal bearing simulation are summarized, the requirements for the simulation approach to fulfil the previously highlighted challenges are explained. Then, the detailed lubricant properties under high pressure and high shear rate are presented. Finally, the layout of the journal bearing test-rig and the simulation model is described which is used for the study on journal bearing friction and wear.

3.1. Requirements for journal bearing simulation

The requirements for a reliable analysis of journal bearing friction and wear can be derived from the challenges described in Section 2.

- High load in a turbocharged and downsized engine deforms the engine parts elastically. Therefore, the elastic deformation needs to be considered in the simulation. For instance, an elastic deformation of the shaft can lead to a misalignment between journal and bearing and this affects the behaviour of the journal bearing. Furthermore, the high pressure in the lubricated contacts deforms the contacting surface which obviously affects the film thickness. Especially, the local elastic deformation of the significantly softer bearing shell—compared to the hardened shaft—needs to be considered.
- Due to the increasing specific pressure in journal bearings the rheological properties of the lubricant at high pressure play an important part. The viscosity of lubricants increases strongly at high hydrodynamic pressures and this piezo-viscous effect must be taken into account. In addition, modern automotive lubricants behave like highly non-Newtonian as a consequence of their complex composition. The effective viscosity varies within the lubrication gap due to locally different hydrodynamic pressures and shear rates. Both effects can have a major influence on the local viscosity in the journal bearing.

- Mixed lubrication and further the prediction of metal-metal contact become more crucial as the minimum film thickness decreases. To reliably predict friction and wear, an accurate description of metal-to-metal contact is required. Consequently, a contact model must be incorporated into the simulation model.
- A realistic description of the surface structure, which means both material and topography, of the journal bearings becomes increasingly important. Not only because journal bearings operate in mixed lubrication more frequently, but also because their surface properties become increasingly refined. Therefore, parameters for the simulation model must be derived from real measured surfaces.
- Any misalignment between journal and bearing can lead to severe metal-metal contact especially at the bearing edge. During the running in of the bearing, the bearing shells are able to adapt their geometry for a better fit between journal and bearing. This geometrical adaption can be larger than the minimum lubrication gap. Therefore, the adapted surface geometry needs to be considered in the simulation as metal-metal contact is largely overestimated otherwise [35, 36].
- The highly nonlinear behaviour of dynamically loaded journal bearings requires a transient calculation in time domain [33]. Especially to understand journal bearing behaviour during the starting and stopping of the shaft, a transient calculation is demanded.
- Thermal effects also change the lubricant viscosity and need to be considered in bearing simulation. In this study, the temperature influence is considered by deriving equivalent temperatures for the isothermal simulation. Of relevance but beyond the scope of this study is the consideration of the local temperature by thermal equations. This will be the focus of future research.
- Finally, the simulation approach needs to be validated by measurement results because approximated functions are used to describe the lubricant or statistically derived contact models are implemented.

3.2. Fundamentals of mixed elasto-hydrodynamic lubrication theory

The fundamental differential equation which describes the lubricant film in a journal bearing is the Reynolds equation. The Reynolds equation together with a suitable cavitation boundary condition and a coupling with the surrounding deformable bodies form the basis of the elasto-hydrodynamic lubrication (EHD) approach. The basic Reynolds equation considers smooth surfaces, but when the distance between the facing surfaces decreases their surface roughness will affect the oil flow. To take this micro-hydrodynamic effect into account, Patir and Cheng [37, 38] introduced flow factors to the Reynolds equation:

$$-\frac{\partial}{\partial x}\left(\phi_x \theta \frac{h^3}{12\eta}\frac{\partial p}{\partial x}\right)-\frac{\partial}{\partial y}\left(\phi_y \theta \frac{h^3}{12\eta}\frac{\partial p}{\partial y}\right)+\frac{\partial}{\partial x}\left(\theta h \frac{u_1+u_2}{2}\right)+\frac{\partial}{\partial x}\left(\theta \phi_s \frac{u_1+u_2}{2}\sigma s\right)+\frac{\partial}{\partial t}(\theta h)=0, \tag{1}$$

http://dx.doi.org/Chapter DOI: 10.5772/64247

where x and y denote the circumferential and the axial direction. p is the hydrodynamic pressure and h is the oil film thickness which depends on x and y. Further, u_1 and u_2 denote the sliding speeds of the facing surfaces. The influence of surface roughness is considered by the pressure flow factors φ_x, φ_y and the shear flow factor φ_s. The oil viscosity η which is a function of x and y is considered to depend on the temperature, pressure and shear rate in this work. Finally, θ represents the fill ratio which is introduced to consider mass conserving cavitation in the model. The cavitation model is based on the Jakobsson-Floberg-Olsson (JFO) approach [39, 40].

If the fluid film cannot completely separate the two contacting surfaces anymore, single asperities interact and metal-metal contact occurs. The contact model according to Greenwood and Tripp [41] is used to estimate the metal-metal contact pressure by the following equation:

$$p_a = KE^* F_{5/2}(H_s), \tag{2}$$

where the composite elastic modulus E^* is a combined material parameter of the contacting surfaces, the elastic factor K depends on surface roughness, asperity radius and asperity density. $F_{5/2}$ is a form factor [35] which is a function of the dimensionless clearance parameter H_S.

The parameters for the contact model used in this study are derived from scans of the bearing surface and the shaft surface. The detailed surface parameters are described in [42, 43].

Friction losses in highly loaded journal bearings consist of hydrodynamic losses only or of both hydrodynamic losses and losses due to metal-metal contact. In this study, the friction losses are represented as friction torque which can be calculated by integrating the hydrodynamic shear stress τ_h and the asperity shear stress τ_a over the bearing surface:

$$M_{Friction} = r \iint_A (\tau_h + \tau_a) dx\, dy. \tag{3}$$

The hydrodynamic shear stress can be calculated by

$$\tau_h = \eta \cdot \frac{u_1 - u_2}{h} (\phi_f \pm \phi_{fs}) \pm \left(\phi_{fp} \frac{h}{2} \cdot \frac{\partial p}{\partial x} \right), \tag{4}$$

where + and − refer to the shell surface and the journal surface, respectively. φ_f, φ_{fs} and φ_{fp} are shear stress factors according to Patir and Cheng [37, 38]. According to the hydrodynamic shear stress the friction torque is proportional to the lubricant viscosity and it is essential to consider detailed lubricant properties to reliably assess friction:

$$\tau_a = \mu_{Bound} \cdot p_a, \tag{5}$$

The asperity shear stress is calculated by multiplying the asperity contact pressure with a boundary friction coefficient μ_{Bound}. In this study, the boundary friction coefficient is assumed to be constant. This simple approximation is able to yield reliable results for a wide range of operation as shown in the result section.

3.3. Lubricant properties at high pressure and high shear rate

The lubricant used in this study is a fully formulated low-viscous 0W20 hydrocarbon engine oil. It is a standard multi-grade lubricant which is available for the automotive market. The main properties of the lubricant are summarized in **Table 1**.

Density at 40°C	832.5 kg/m^3
Dynamic viscosity at 40°C	37.5 mPa s
Dynamic viscosity at 100°C	6.8 mPa s
HTHS-viscosity at 150°C and shear rate 10^6 1/s	2.7 mPa s

Table 1. Basic properties of the tested 0W20 lubricant.

The main lubricant properties show that the viscosity is strongly dependent on temperature. Various mathematical functions exist to consider the temperature dependency in simulation. In this study, the effect of temperature on viscosity is specified by the Vogel equation [44] which is very accurate for hydrocarbon lubricants,

$$\eta(T) = A \cdot e^{B/(T+C)}. \tag{6}$$

where T is the oil temperature and A, B and C are constants for a given lubricant. In dynamically loaded journal bearings, high pressures above 2000 bar can occur and the increase of viscosity can be very significant. Consequently, the viscosity increase with high pressure needs to be considered. Here, the simple Barus equation [45] is utilized which only requires the identification of a pressure viscosity coefficient α:

$$\eta(T, p) = \eta(T) \cdot e^{\alpha p}. \tag{7}$$

Due to the dynamic load and high operational speed, shear rates above 2×10^7 1/s can occur in journal bearings. At these conditions, a significant drop in viscosity can be identified. To describe the shear thinning effect, the Cross equation [46] is used:

$$\eta(T, p, \dot{\gamma}) = \eta(T, p) \cdot \left(r + \frac{1 - r}{1 + (K\dot{\gamma})^m} \right). \tag{8}$$

http://dx.doi.org/Chapter DOI: 10.5772/64247

where *K*, *r* and *m* are coefficients for a given lubricant. All coefficients for Vogel, Barus and Cross equation are derived from measured rheological data of the investigated lubricant. The detailed derivation can be found in [47]. The values of the introduced coefficients are listed in **Table 2**.

A	0.0516 mPa s
B	1127.6°C
C	130.7°C
α	0.00095 1/bar
r	0.53
m	0.79
K	7.9×10^{-8} s

Table 2. Parameters for the rheological model of the lubricant.

The viscosity characteristics obtained from the derived parameters are also shown in **Figures 1** and **2**.

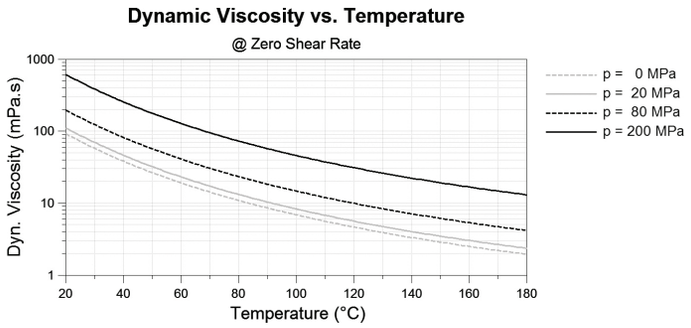

Figure 1. Viscosity-temperature dependency for the 0W20 lubricant at different pressures [48]; please note the logarithmic scale.

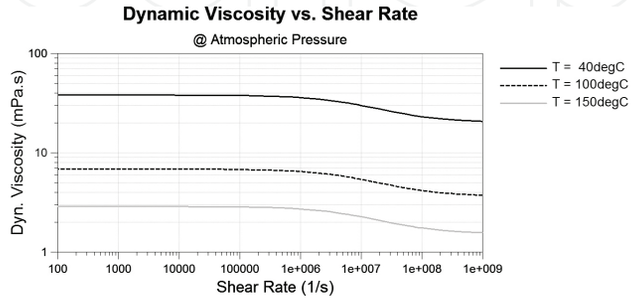

Figure 2. Viscosity-shear rate dependency for the 0W20 lubricant at different temperatures [48]; please note the logarithmic scale.

3.4. Journal bearing tests and the corresponding simulation model

Experimental results are used extensively in this study to validate the presented simulation approach. The experimental part is not the central topic of this work. Therefore, only a brief description of the journal bearing test-rig is provided. More details about the test-rig and the measurement equipment can be found in [43, 47, 49].

All tests are conducted on the journal bearing test-rig at KS Gleitlager[1] as shown in **Figure 3**. The test-rig enables a detailed analysis of journal bearing behaviour under static and dynamic loads for constant or transient shaft speed. The test-rig consists of a straight shaft (test shaft) which rests on two support brackets. Each support bracket contains a plain journal bearing and is fixed on a base. The test connecting rod with the test bearing is placed in between the two support brackets. An external load is applied onto the test connecting rod which is generated by an electromechanical high-frequency pulsator. The test shaft is driven by an elastically clutched electric motor.

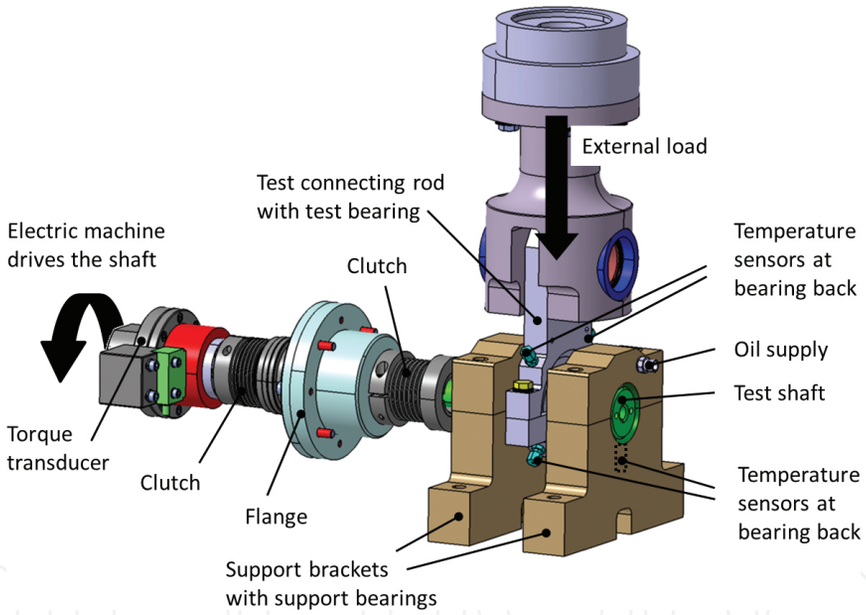

Figure 3. Configuration and components of the journal bearing test-rig [43].

The dimensions and oil supply design of the support bearings correspond to automotive main bearings with a 180° oil supply groove. The support bearings have a diameter of 54 mm and a width of 25 mm. The test journal bearing corresponds to a big-end bearing having an oil supply hole in the load-free (lower) shell. It has a diameter of 47.8 mm and a width of 17.2 mm.

The total friction torque caused by all three journal bearings is measured by a torque transducer which is located between the motor and the clutch.

[1] KS Gleitlager GmbH, Am Bahnhof 14, 68789 St. Leon-Rot, Germany.

http://dx.doi.org/Chapter DOI: 10.5772/64247

For the simulation, the test-rig is modelled within the flexible multi-body solver AVL Excite Power Unit.[2] The multi-body simulation model consists of flexible bodies and joints which connects the bodies. The two support brackets with the support bearings and the test connecting rod including the test bearing are represented as mathematically condensed finite element (FE) structures [50]. Therefore, a pre-processing step needs to be performed with an FE solver to create the condensed bodies. The test shaft is also represented as elastic body but instead of using a condensed structure a simplified beam and disc body is generated.

The lubricated contacts between the test shaft and support bearings as well as between the test shaft and test bearing are modelled as elasto-hydrodynamic joints. The fluid film is calculated according to the averaged Reynolds equation discussed in the previous section (Eq. (1)). The numerical approach requires a discretization of the bearing surface. Therefore, 25 hydrodynamic (HD) nodes are defined in axial direction which are equally distributed in each bearing (support bearings and test bearing). The test bearing has 200 nodes in circumferential direction and the support bearings have 176 nodes. Every second HD node is directly coupled to the condensed FE model.

Because of the high nonlinearity of the model it is solved in the time domain using numerical time integration [33].

3.5. The consideration of temperature in the isothermal simulation method

The numerical approach assumes an isothermal bearing which means that the bearing temperature and the temperature of the lubricant are assumed to be constant in the lubrication gap. Certainly, the temperature changes under different operating conditions, for example, with varying shaft speed and bearing load. To consider the load- and speed-dependent temperature, an equivalent temperature is defined which is derived from measured temperatures at the back of the bearing shell (see sketch of the test-rig in **Figure 3**). Hence, an isothermal bearing simulation is performed while the temperature influence due to different operating conditions is still considered.

The background for this approach was introduced by previous research results from Allmaier et al. [51]. The authors investigated the thermal processes of journal bearings under high dynamic loads and compared the results with experimental data. It was shown that it is possible to predict the measured temperatures at the bearing shell with a complex thermo-elasto-hydrodynamic (TEHD) simulation approach. From these results, a simple equivalent bearing temperature relation was derived for the isothermal EHD simulation that is capable to predict the friction losses very accurately for a large range of different lubricants, journal speeds and loads as was shown in direct comparison to experimental data (see, in particular, [35] and [52], which is available online at www.intech.com[3]). This approach was initially suggested for main bearings with a distinct oil supply groove and was furthermore adapted to bearings with an oil supply hole in [47].

[2] AVL List GmbH, Advanced Simulation Technology, Hans-List-Platz 1, 8020 Graz Austria, www.avl.com.

[3] http://dx.doi.org/10.5772/51568.

4. Simulation results

In the result section, the behaviour of journal bearings under different operating conditions is discussed. Primarily, the bearings are excited with a dynamic load and they operate in the elasto-hydrodynamic lubrication regime. The elastic deformation and also the viscosity under high pressure and shear rate must be considered for a reliable prediction of friction and wear. Furthermore, severe metal-metal contact is generated by a static load and low shaft speed. This condition allows for the verification of the simulation approach in mixed lubrication regime. The presented results give an overview of current research by the authors. The majority of the results are taken from recent publications and, therefore, we refer to the original publications for further reading [42, 43, 47, 48, 53].

4.1. Impact of high pressure and shear thinning on journal bearing friction

The first application example discusses friction in dynamically loaded journal bearings. The bearings operate in the elasto-hydrodynamic regime with only a minor metal-metal contact. Due to the heavy load, maximum hydrodynamic pressures above 200 MPa arise in the bearings. At shaft speeds of up to 7000 rpm, high shear rates occur, which induce a noticeable drop of viscosity as will be shown.

To reliably predict friction in this condition a detailed description of the lubricant behaviour under high pressure and high shear rate becomes absolutely necessary. The influence of neglecting the piezo-viscous effect and the non-Newtonian behaviour on the accuracy of friction prediction in journal bearings is demonstrated.

4.1.1. Journal bearing conditions

Two dynamic load cases are investigated in this first study, one with a maximum external load of 40 kN and a second one with 80 kN. The dynamic characteristic of the load during a full load cycle is shown in **Figure 4**.

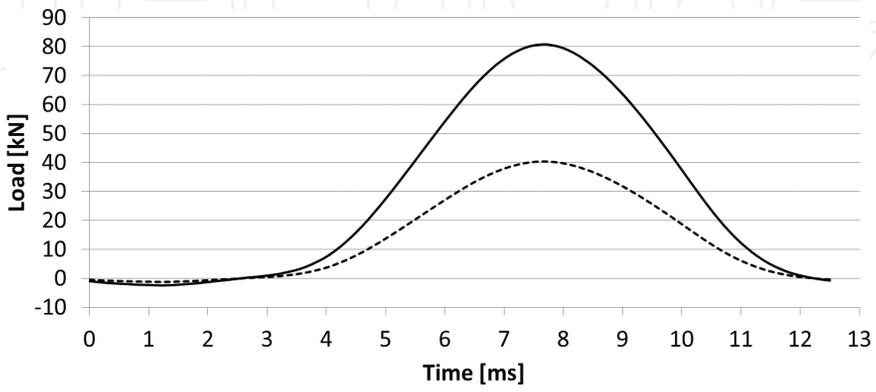

Figure 4. Dynamic load applied to the test bearing [47].

http://dx.doi.org/Chapter DOI: 10.5772/64247

The maximum specific loads in the test bearing which is the maximum load related to the projected bearing area, correspond to 50 MPa (40 kN load) and 100 MPa (80 kN load). The operational shaft speed starts at 1000 rpm and runs up to 7000 rpm with 1000 rpm increments. Each step is operated for 20 minutes. The run-up is followed by a run-down back to 1000 rpm. These conditions cover a wide range of operating conditions which are also typical for combustion engines.

4.1.2. Verification of the simulation results and the importance of the lubricant model

The figures in this section show a comparison of the simulation results and the measurement results. The simulation results are obtained with three different lubricant models. The results are arranged in such a way that the importance of lubricant properties in the elasto-hydrodynamic journal bearing simulation is highlighted. Therefore, we start with the simplest lubricant model $\eta(T)$ which is only dependent on temperature. Afterwards the piezo-viscous effect is added to the lubricant model $\eta(T,p)$ and, finally, the complete lubricant model also considers the shear thinning effect $\eta(T,p,\dot{\gamma})$.

Figure 5 shows the measured and calculated mean friction torque over shaft speed for the two different loads. The dashed lines represent the measured data. The error bars show the uncertainty which contains the error of the torque transducer and the standard error of the mean. As expected, the friction torque rises with increasing shaft speed and also with higher load. The influence of temperature can be clearly seen by comparing the 100 MPa results during the run-up and the run-down. At the run-down the bearing temperature is consistently 3°C higher compared to the run-up. Due to the lower viscosity at higher temperature, this small temperature difference reduces the friction torque by about 0.2 Nm.

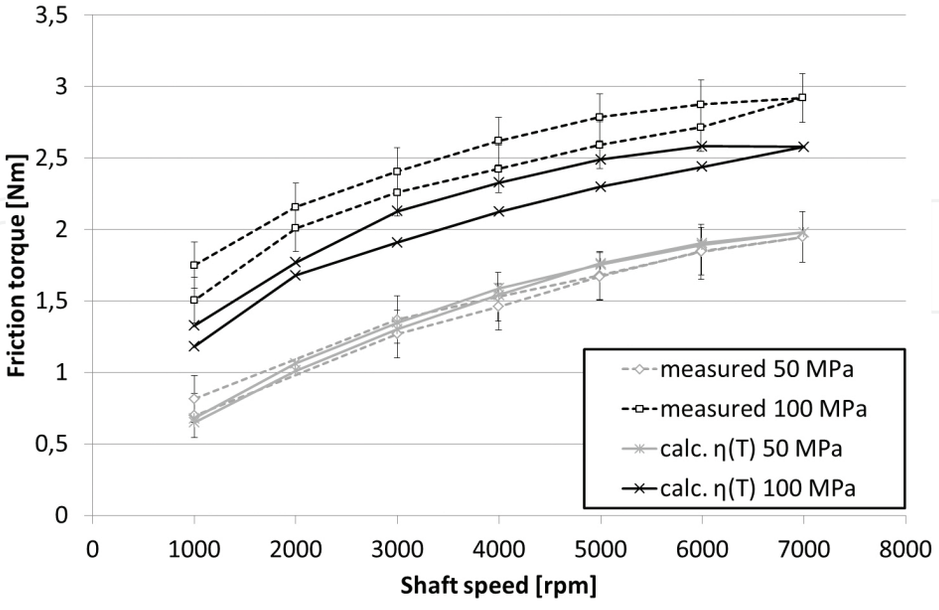

Figure 5. Comparison of the average friction torque measured on the test-rig with the simulated mean friction torque using the basic oil model $\eta(T)$ at 50 and 100 MPa specific loads [47].

The calculated average friction torque using the simple temperature-dependent viscosity model $\eta(T)$ is shown by solid curve in **Figure 5**. While the calculated friction torques at 50 MPa agree closely to the measured curve, the calculated friction torques at 100 MPa underestimate the measured torques over the entire speed range. However, the difference due to higher temperature at the run-down has been correctly identified. This indicates that the temperature consideration for the isothermal bearing calculation performs as intended.

The simulation results allow for a greater insight into the film formation and the occurring hydrodynamic pressure. At a specific load of 100 MPa a peak oil film pressure of around 200 MPa in the test bearing is identified independently from the shaft speed. As can be seen in **Figure 1**, the pressure-induced viscosity increase is significant for such high pressures. Consequently, the lubricant viscosity increases nearly sevenfold compared to the viscosity at ambient pressure. Therefore, calculations using the pressure-dependent oil model $\eta(T,p)$ are performed and the results are shown as solid curves in **Figure 6**.

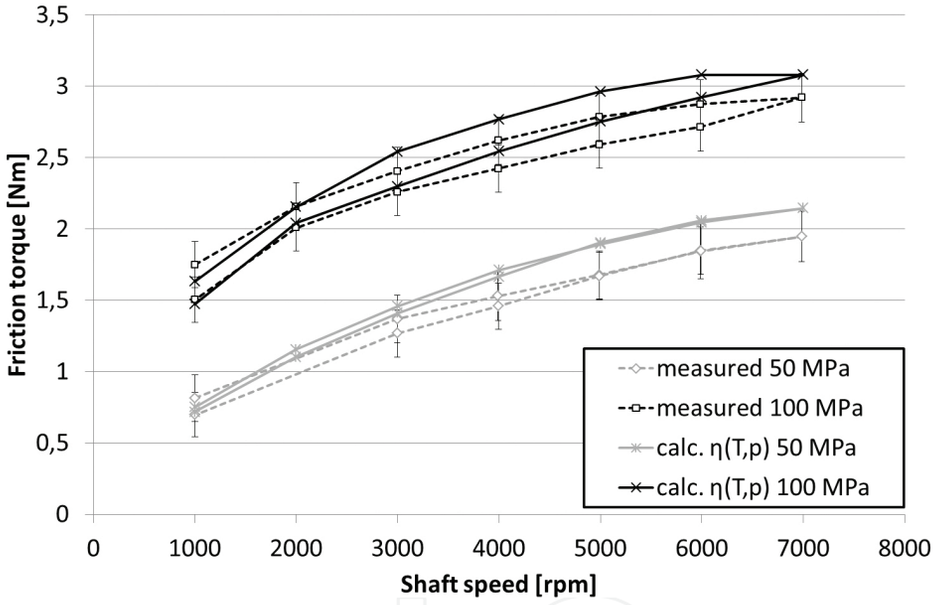

Figure 6. Comparison of the average friction torque measured on the test-rig with the simulated mean friction torque using the pressure-dependent oil model $\eta(T,p)$ at 50 and 100 MPa specific loads [47].

The friction torque increases for all operating conditions when considering the pressure-dependent oil model. The impact of the piezo-viscous effect depends on the applied load and is as expected, more relevant for the 100 MPa load than for the 50 MPa load. At low shaft speeds, the calculated friction torque agrees closely with the measured torque results for both the load cases. However, for shaft speeds above 3000 rpm the calculated torque overestimates increasingly the measured torque.

The relative sliding speed between shaft and bearing increases with higher shaft speed and, hence, higher shear rates occur. The shear rate increases nearly linearly with the shaft speed and reaches a maximum of 2.2×10^7 1\s at 7000 rpm [47]. At high shear rate like this, the viscosity drop due to the shear thinning effect is significant. For the studied lubricant a

http://dx.doi.org/Chapter DOI: 10.5772/64247

reduction of 25% is obtained (compare **Figure 2**). Finally, the results calculated with the complete oil model $\eta(T,p,\gamma;)$ are shown in **Figure 7**.

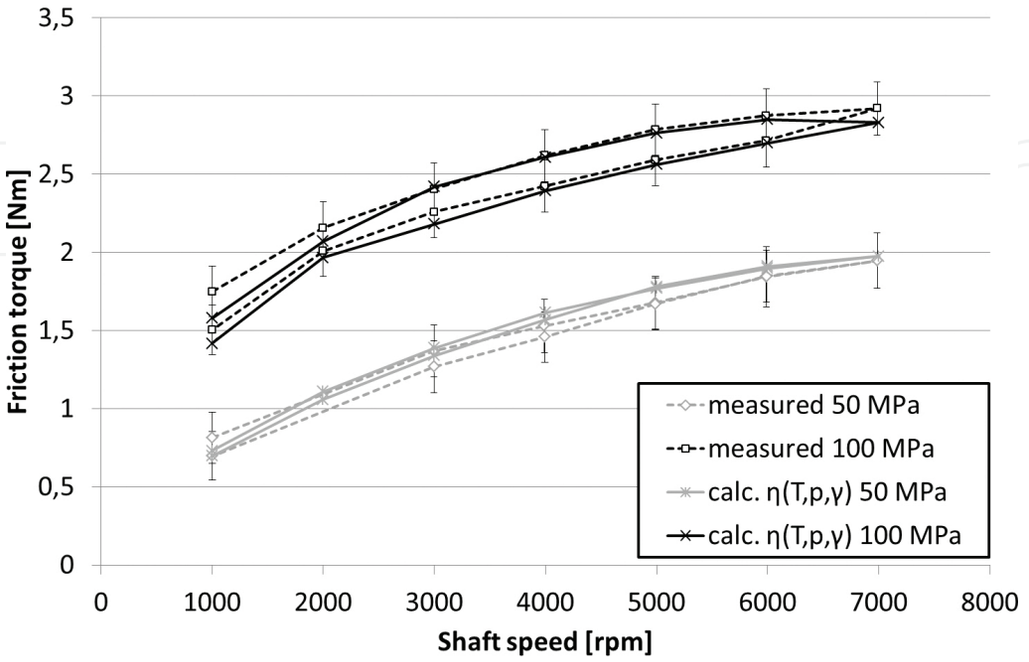

Figure 7. Comparison of the average friction torque measured on the test-rig with the simulated mean friction torque using the complete oil model $\eta(T,p,\gamma;)$ at 50 and 100 MPa specific loads [47].

As the shear rates increase with the shaft speed, the influence of the shear thinning effect is very small at low shaft speeds and becomes increasingly important for higher shaft speeds. At 1000 rpm the maximum shear rate is smaller by a factor of 10 compared to 7000 rpm. As a consequence, the influence of shear thinning on the friction torque is almost negligible for low shaft speed. The effect of shear thinning reduces the calculated friction torque particularly at high shaft speed. Above 5000 rpm, a torque difference of about 0.15 Nm is determined between the two lubricant models $\eta(T,p)$ and $\eta;(T,p,\gamma;)$ independently of the load case.

To summarize the first example, the calculated friction torques considering temperature-, pressure- and shear-rate-dependent viscosity match the measured friction torques within the measurement uncertainty for both the run-down and the run-up. A deviation may be identified at low shaft speeds during the run-up. It is important to note that new journal bearings are used for each test run. And therefore the journal bearing experiences a run-in process in the beginning of its operation. An adaption of the bearing surface in particular at the bearing edges takes place which causes higher friction losses during this time. The simulation considers already run-in bearings by including this adapted surface geometry. Consequently, differences between the measured and simulated results arise. This run-in process happens during the first and second step (1000 and 2000 rpm), when the measured friction torque is accordingly higher compared to the calculated friction torque. The wear process due to the run-in is discussed in more detail in the following example.

4.2. Edge loading and running-in wear in dynamically loaded journal bearings

After the friction tests under dynamic loading (see Section 4.1), the bearing shells were analysed and a worn region was identified at the bearing edges. In Section 4.1, these worn regions are considered in the simulation right from the start instead of a perfect cylindrical bearing surface. In this section, the worn surface geometry is calculated in a stepwise process by iteratively removing material from the initial perfect cylindrical bearing shell.

4.2.1. Running-in caused by edge loading and iterative wear calculation

When two contacting elements operate together for the first time, adaptions of their surfaces occur. These adjustments concern the geometrical conformity on both the macro- and micro-scale as well as changes of the mechanical and material properties [54]. Such an adjustment process takes place in the early stage of operation and is commonly called running-in. In hydrodynamic journal bearings a geometrical unconformity is caused by any misalignment between shaft and bearing shell. This unconformity originates from production tolerances, assembly deformation or thermal deviation. In this study, the applied heavy load bends the shaft elastically which leads to a misalignment and further, to metal-metal contact at the bearing edges. The principal manner is sketched in **Figure 8** on the left. In hydrodynamic journal bearings the softer shell generally adapts its surface to fit the harder journal during the running-in. When the running-in process has finished, metal-metal contact in the lubrication gap vanishes completely.

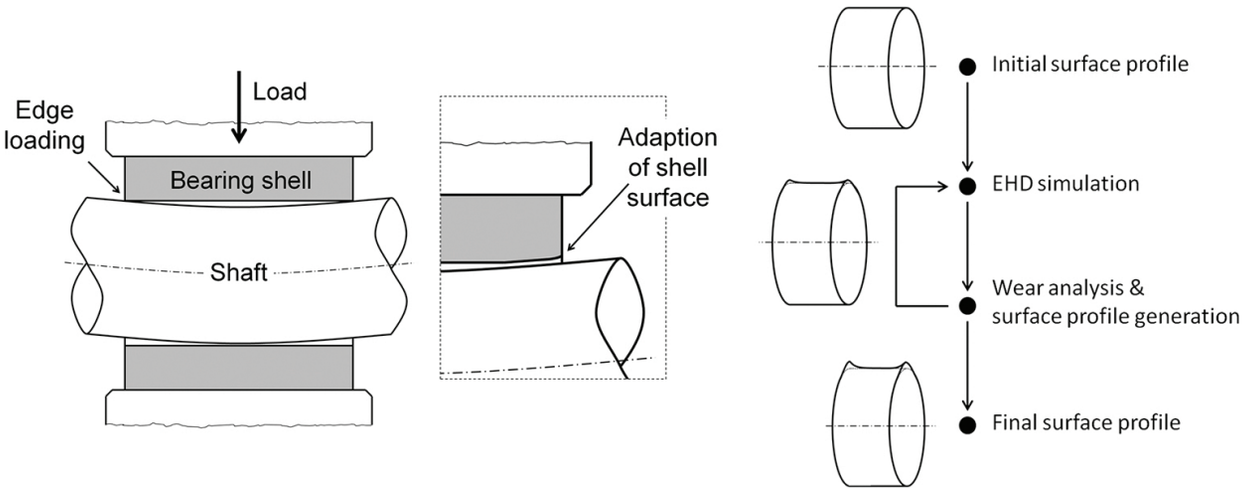

Figure 8. Edge loading caused by elastic bending of the shaft; the flowchart of the iterative surface profile generation on the right [42].

Figure 8 (right) shows the iterative scheme of the wear calculation. By starting from the initial perfectly cylindrical bearing shape of a new bearing, the wear equation from Archard [55] is used to calculate the wear depth for all HD nodes of the discretized journal bearing surface. Archard's wear equation can be written as

http://dx.doi.org/Chapter DOI: 10.5772/64247

$$h_w = \frac{C}{H} \cdot W \cdot L = \frac{C}{H} \cdot t_{Step} \cdot \overline{W_L}, \tag{9}$$

where h_w denotes the wear depth, W the normal load, L the sliding distance, C the wear coefficient and H describes the hardness of the contact surface. The product of normal load and sliding distance can be substituted by a step time t_{Step} multiplied with a wear load W_L. The wear load is the averaged product of asperity contact pressure and relative sliding speed over a load cycle and is different for each (discretized) spot of the bearing surface.

In this wear process a maximum wear depth per iterative step is defined which is generated at the HD node with a maximum wear load. The wear depth of all other HD nodes can then be calculated and a new surface profile is generated. Additionally, the time required to achieve the worn geometry and the overall wear volume can be calculated for every step. With this adapted bearing surface another full elasto-hydrodynamic simulation step is started and the wear calculation is performed again. This process is repeated until the mixed lubrication, or more precisely the maximum asperity contact pressure, becomes insignificantly small. Wear on the journal surface is neglected because of the significantly higher hardness compared to the bearing shell surface.

Central to the wear analysis is the contact model which evaluates the metal-metal contact pressure according to the film thickness in the bearing. To reliably describe the contact pressure, the roughness parameters of the contact model need to be obtained from the real surfaces. Hence, the shaft and bearing shell surfaces are scanned and analysed. For a detailed derivation of the roughness parameters see [42].

4.2.2. Results of the iterative wear simulation

The running-in procedure is calculated for a shaft speed of 4000 rpm and a maximum specific load of 100 MPa (see previous example). Starting point of the wear process is the definition of the initial (cylindrical) journal bearing shape followed by an EHD simulation of a full load cycle. Metal-metal contact is observed when the applied load reaches its maximum. The test bearing in particular shows metal-metal contact at both bearing edges. The symmetrical appearance of the metal-metal contact is caused by the symmetric bearing layout and the according deflection curve of the shaft. **Figure 9** shows the distribution of the calculated metal-metal contact pressure on the left.

Subsequently, the wear load during a full load cycle is calculated and the worn surface geometry is generated. The generated profile is then used as bearing geometry in the subsequent simulation step. As a result, a reduction of the maximum metal-metal contact pressure is obtained. When the procedure is repeated 40 times, as show, it can be observed that the maximum metal-metal contact pressure gradually decreases. The evolution of the maximum contact pressure during the iterative process is shown in **Figure 9** (right). The stepwise pressure reduction is significant in the beginning of the wear process but becomes smaller from step to step. The step time to achieve the defined maximum wear depth per iterative step is also shown in **Figure 10**. The step time monotonically increases from 2.5 to 1050 s.

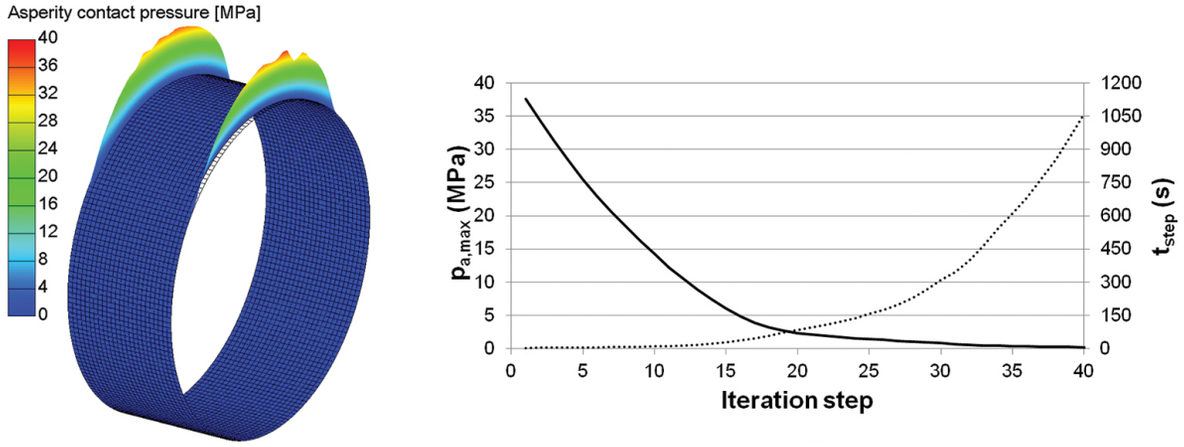

Figure 9. Calculated asperity contact pressure for the first step at the point of maximum load on the left; development of maximum asperity contact pressure and step time over the number of iterative steps [42].

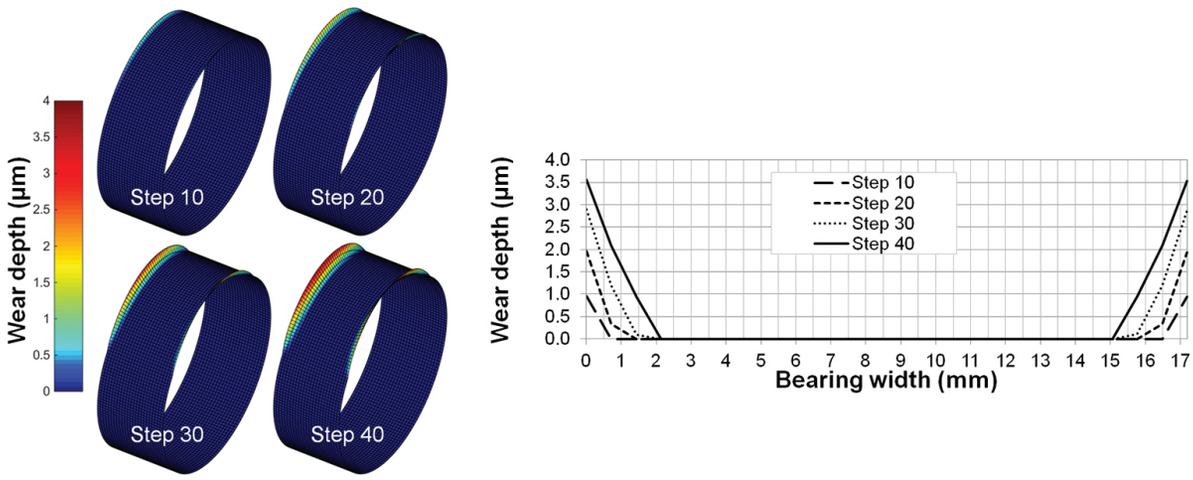

Figure 10. Surface profile on the left and a section view of the surface profile during the iterative running-in process at the position of maximum wear depth on the right [42].

Figure 10 shows the development of the surface profile for the test bearing. Wear concentrates on the edges of the upper bearing shell and shows a symmetrical appearance. With a higher number of iterative steps the worn area expands in axial and circumferential direction. And also the wear depth at the edges increases gradually and reaches a maximum of 3.6 µm after 40 steps.

Finally, the maximum metal-metal contact pressure and the wear volume are plotted over the time in **Figure 11**. Within the first 200 s of operation the maximum contact pressure drops sharply below 5 MPa. From there on the maximum asperity contact pressure steadily decreases to a minimum in the end. The wear volume strongly increases in the beginning and flattens out over time. A steady state of wear has not been identified during the investigated time period.

http://dx.doi.org/Chapter DOI: 10.5772/64247

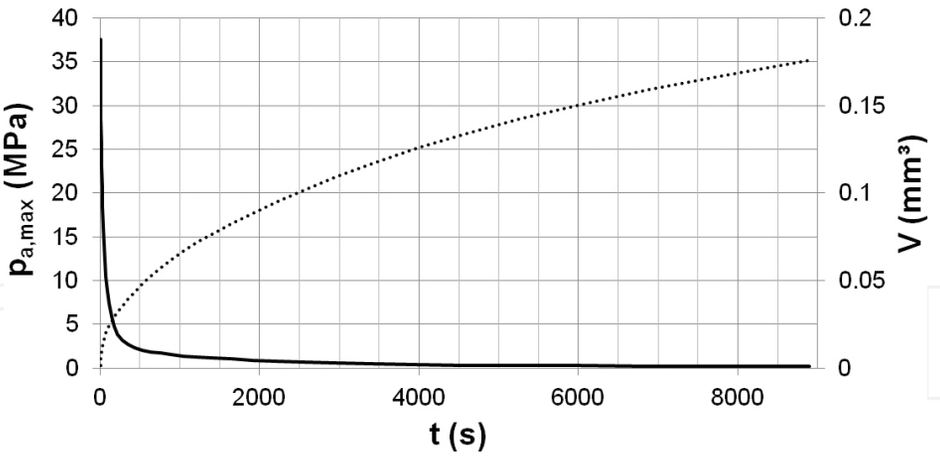

Figure 11. Maximum asperity contact pressure and the accumulated wear volume over time [42].

The quick reduction of asperity contact pressure in the beginning of the bearing operation verifies the statement from the previous example in Section 4.1: at low shaft speeds during the run-in a deviation between the measured and calculated friction torque was identified. This is caused by additional friction losses due to metal-metal contact of the run-in process. Metal-metal contact did not occur in the simulation because an already worn surface geometry was assumed.

In this section, the simulation of the wear process yielded a calculated final surface geometry that is a good match to the worn surface of the test bearing obtained after the dynamic tests. The comparison of wear depth as well as the extent of the worn area shows that the presented method is able to predict the worn surface geometry in highly stressed journal bearings (detailed comparison see [42]).

This section has also shown that the running-in process concentrates on rather small areas of the journal bearings and, therefore, metal-metal contact occurs only locally. The small amount of metal-metal contact only marginally affects the friction losses in the bearing. Hence, the investigated dynamical load is not well suited to analyse friction in the mixed lubrication regime. Consequently, the next section studies the mixed lubrication regime up to severe metal-metal contact.

4.3. Simulation of journal bearing friction in severe mixed lubrication

In the mixed lubrication regime, metal-metal contact occurs and becomes dominant which leads to a drastic rise in friction. Texture and roughness of the bearing surface has a major influence on friction in the mixed lubrication regime. In the simulation, the bearing surface is represented by the contact model which is responsible to reliably predict metal-metal contact pressure as well as contact area.

This section experimentally verifies the relatively simple simulation approach using Greenwood and Tripp contact model in combination with a constant friction coefficient. The input data for the contact model are derived from surface scans of the bearing. Furthermore, the influence of surface roughness on friction is discussed.

4.3.1. Journal bearing conditions and experimental details

To ensure the occurrence of metal-metal contact on the bearing test-rig and in contrast to the previous sections, a static load is applied to the test bearing. The tests start at high shaft speed and the shaft speed is slowly reduced to enable the journal bearing to enter the mixed lubrication regime. The results are represented by Stribeck curves that allow an identification of the different lubrication regimes, as shown in **Figure 12**. The Stribeck curve shows the friction torque over the shaft speed. The transition between the hydrodynamic lubrication regime and the mixed lubrication regime can be identified by a strong increase of the friction torque.

Two load cases are investigated in this section, the first with 8 kN static load and the second with a 4 kN load, which correspond to 10 MPa and 5 MPa specific load in the test bearing, respectively. In the beginning of each test, new bearing shells are placed into the test connecting rod and the support brackets. One test run consists of a constant speed-up to 6000 rpm followed by a constant speed-down until the shaft stops to rotate. One test run lasts for 12 min. Only the speed-down is recorded and evaluated.

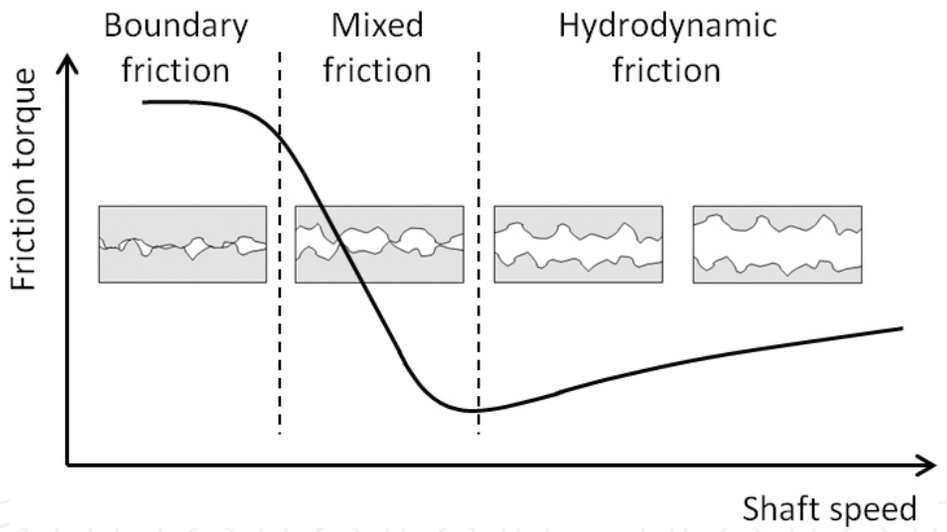

Figure 12. Sketch of a Stribeck curve with different lubrication regimes [43].

Surface	New	Worn
R_a (μm)	0.27	0.22
R_q (μm)	0.34	0.26
σ (μm)	0.28	0.23
δ (μm)	0.39	0.19

Table 3. Surface roughness and simulation input parameters for the contact model.

http://dx.doi.org/Chapter DOI: 10.5772/64247

The bearing surface is scanned by a white light interferometer and the input parameters for the contact model are derived. For evaluating the influence of surface roughness, the bearing shell is measured before the test run and a worn bearing shell is scanned too. The main properties are summarized in **Table 3**. The arithmetic average R_a of the bearing shell surface decreases from 0.27 μm for the new bearing to 0.22 μm for the worn bearing. A similar decrease can be seen for the root mean square R_q, which is 0.34 μm for the new and 0.26 μm for the worn bearing. The asperity summit roughness σ and the mean summit height δ are relevant for the contact model. Additional details about the contact model can be found in [43]. In contrast to the previous example, a cylindrical geometry of the journal bearings is considered in the simulation. The difference between the new and the worn surface only concerns the surface roughness parameters.

Beside the parameters for the contact model, a suitable boundary friction coefficient that considers the presence of friction modifying additives [56] is required to predict friction. Here, the boundary friction coefficient is chosen to be constant $\mu_{\text{Bound}} = 0.02$. The limits of this simplification are discussed in the results.

4.3.2. Verification of the simulation results and the influence of surface roughness

Figure 13 shows a comparison of the simulation results and the measurement results. On the left the results for the 8 kN load and on the right for 4 kN are presented. The dashed line shows the measurement results and the grey area indicates the uncertainty band of torque and speed measurement.

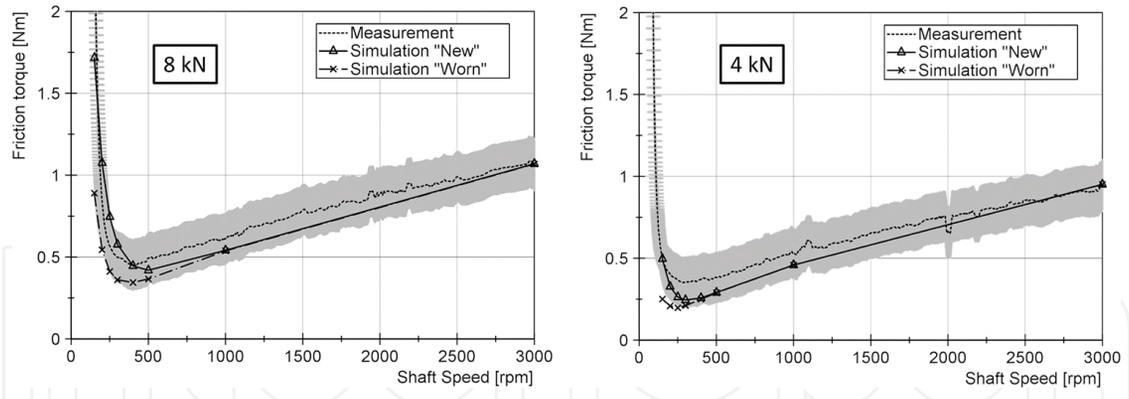

Figure 13. Comparison between the calculated and measured friction torque over shaft speed at a load of 8 and 4 kN [43].

At maximum shaft speed the bearing operates in pure hydrodynamic lubrication regime and a friction torque of about 1.1 Nm arise for the 8 kN load. By reducing the shaft speed the friction torque decreases to a minimum at around 400 rpm. Below 400 rpm the bearing operates in mixed lubrication regime and the friction torque increases abruptly. Similar behaviour can be seen at a load of 4 kN. In the hydrodynamic regime the friction torque is 0.15 Nm lower compared to the 8 kN load and also the transition between hydrodynamic and mixed lubrication regime is shifted to a lower shaft speed.

The two other curves represent the calculated friction torque with the new bearing surface roughness (solid curve) and the worn bearing surface roughness (dashed curve). In the hydrodynamic lubrication regime both surfaces predict identical friction torques. A difference can be seen at low speed, when the new bearing surface predicts an earlier increase of friction torque compared to the worn surface. However, at 8 kN load the results calculated with both surfaces lie within the measurement uncertainty but regarding the transition speed the calculation with the worn surface appears to be more suitable. At 4 kN the results with the new surface match the transition speed.

It can be expected that a modification of the surface roughness occurs at the beginning of the operation. As mentioned earlier, a speed-up is performed before the measurements take place. During the speed-up metal-metal contact already occurs and the surface may smoothen already. For a higher load more metal-metal contact develops and a quicker surface modification can be expected. The quicker adaption at 8 kN load eventually explains the good match of measurement and simulation with the worn surface roughness.

The comparison of measurement and simulation shows a good agreement in hydrodynamic lubrication regime and mixed lubrication regime. Hence, the presented roughness data observed from surface scans in combination with the simple contact model are suitable for the friction prediction in journal bearings operation under severe conditions. Also, the chosen constant friction coefficient μ_{Bound} is suitable for both loads to predict friction with a great accuracy. Only at a very low shaft speed when the bearing operates in boundary friction regime, the friction torque is underestimated. Here, a higher boundary friction coefficient would be more applicable.

4.4. Friction analysis of journal bearings during starting and stopping

A transient start-stop simulation is performed in the final example. The journal rests in the bearing in the beginning of the simulation. When the journal starts to rotate the breakaway torque has to be overcome. Afterwards, the bearing operates in mixed lubrication regime until the lift-off speed is reached.

4.4.1. Experimental details and journal bearing resting conditions

A static load of 2.5 kN is applied to the test connecting rod. The resting test shaft is constantly accelerated to a maximum speed of about 260 rpm. The duration of the speed-up is 3 s. Subsequently, the shaft is constantly decelerated over 3 s until the shaft stops. This start-stop cycle was repeated 6000 times. In between each cycle was a recovery phase of 3 s.

The simulation model from previous examples is modified in a way that the shaft follows a predefined rotation to analyse the start-stop behaviour. The parameters for the contact model and the boundary friction coefficient remain unchanged. However, before the shaft starts to rotate a static condition needs to be established. Therefore, an initialization phase is included where the static load is gradually applied to the bearing and the shaft moves slowly towards the bearing shell until it reaches its resting position. **Figure 14** (left) shows the bearing force and the minimum film height in the lubrication gap.

http://dx.doi.org/Chapter DOI: 10.5772/64247

During the first 0.1 s, the static load is constantly increased until 2.5 kN is reached. At the beginning of the initialisation phase, the shaft is located at the centre of the bearing. As the load increases the shaft subsides within the bearing and the minimum radial distance between shaft and bearing (minimum film height) decrease. After 0.3 s, the minimum distance is reached. At resting position, the journal is mainly supported by metal-metal contact which can be seen in **Figure 14** (right). While the test bearing shows an equally distributed contact pressure all along the bearing axis, the support bearing show an asymmetric distribution. This asymmetric distribution is caused by the elastic deformation of the shaft due to the static load (deflection curve). The actual starting of the shaft happens after 0.5 s. The shaft is then accelerated and decelerated again until the shaft completely stops to rotate.

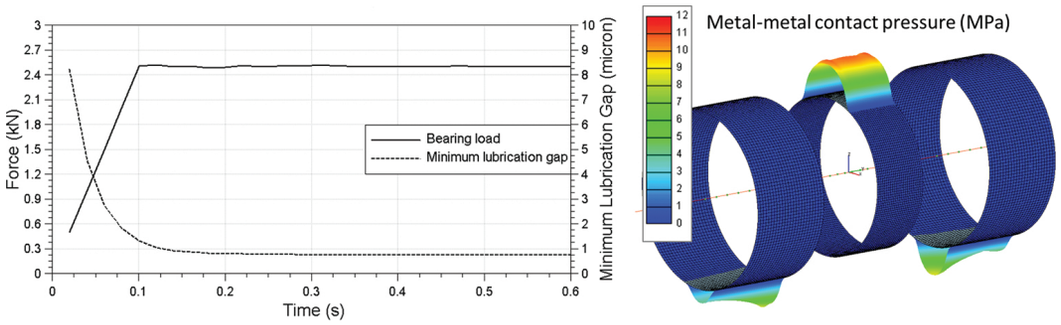

Figure 14. Load of the test bearing and minimum film height during the initial phase of the start-stop cycle on the left; metal-metal contact pressure distribution after 0.5 s in the test bearing and the two support bearings [53].

4.4.2. Verification of the simulation results and the influence of surface roughness

The measurement and simulation results are summarized in **Figure 15**. The dashed black curve shows the rotational speed of the shaft; it reaches a top speed of 260 rpm. The solid black curve represents the measured torque. The results were taken from the 3000th cycle and, therefore, a running-in of the bearing has already occurred. Shortly before the shaft begins to rotate the torque abruptly increases to a maximum. This peak, or breakaway torque, indicates the transition between static and sliding friction. Once in motion the bearing enters the mixed lubrication regime and the friction torque decreases quickly. After 1.5 s, the friction torque becomes a minimum as the bearings enter the hydrodynamic lubrication regime. At stopping the measured torque does not show any increase until 6.2 s when the recording of the data ended. The measured signal shows strong fluctuations which are caused by the dynamic behaviour of the test-rig. It can be expected that the impulse at the breakaway cause this strong fluctuations. Bouyer and Fillon [57] observed a similar behaviour and referred to the slip-stick phenomenon.

The solid grey curve shows the calculated torque considering a new bearing surface. When the shaft starts to rotate, it raises identically with the measured friction torque. Also the magnitude of the breakaway torque is equal to the measured one. After the breakaway both curves drop parallel as they reach mixed lubrication. The hydrodynamic regime is reached after 2 s. In the end of the start-stop cycle the simulation predicts an increase of friction torque

before the shaft completely stops. The fluctuations are not present in the simulation because the rotational speed of the shaft is specified.

Similar to the previous result section, the influence of surface roughness is analysed by simulation. The friction torque calculated with a worn surface roughness is shown as dashed grey line in **Figure 15**. The breakaway torque remains unchanged compared to the results with the new bearing surface because at rest the shaft is completely supported by metal-metal contact and, hence, the breakaway torque is only defined by boundary friction coefficient, μ_{Bound}. In the mixed lubrication regime, the friction torque reduces quickly and pure hydrodynamic lubrication is reached after 1.5 s. At top speed both surface roughnesses yield a similar torque in the simulation. A major difference can be seen in the behaviour during the slowdown and the stopping of the shaft. The calculation with the worn bearing surface roughness shows a clear reduction of maximum friction torque which also fits better with the measured friction torque.

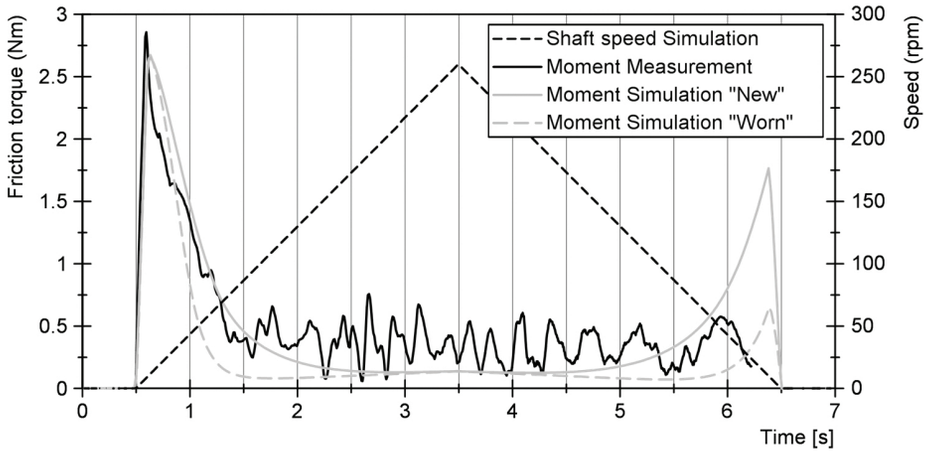

Figure 15. Measured and calculated friction torque during a start-stop cycle; results from simulation are obtained for new and worn bearing surface roughness [53].

Overall, the calculated friction torque follows the starting and stopping behaviour of the shaft in the bearing very closely. Especially the breakaway torque and the transitions between the boundary and mixed lubrication regime as well as between the mixed and hydrodynamic lubrication regime are identified. The model considering the new bearing surface roughness overestimates the friction torque during stopping of the shaft.

5. Conclusion and outlook

This chapter analyses the behaviour of automotive journal bearings under severe loading conditions. The severe loading conditions force the bearing to operate in the boundary, mixed and elasto-hydrodynamic lubrication regime. Therefore, an extensive simulation approach is employed which considers elastic deformation of the components, the rheological properties of the lubricant under high pressure and at high shear rate, and a contact model to calculate

http://dx.doi.org/Chapter DOI: 10.5772/64247

metal-metal contact. Both the lubricant properties and the surface roughness parameters for the contact model are experimentally identified. The simulation approach is comprehensively validated on the basis of measurements on a journal bearing test-rig.

The first example shows the importance of considering the piezo-viscous and the non-Newtonian effect of the lubricant to reliably predict friction in highly loaded journal bearings. If both the effects are neglected, a discrepancy of up to 15% can occur in comparison to the measured results for the studied operating conditions. The second example discusses the running-in behaviour of misaligned journal bearings which is caused by the elastic bending of the shaft. Therefore, an iterative simulation approach is presented which removes material from the bearing shell step by step. Friction in mixed lubrication is analysed in the third example where the Stribeck curves are calculated and compared to the measured results. The influence of surface roughness on mixed friction is investigated. Finally, a transient start-stop cycle is calculated in the fourth example. Before the shaft starts to rotate, a breakaway torque has to be surmounted. The bearing shortly operates in mixed lubrication before the contacting surfaces are completely separated. Especially at the stopping of the shaft an influence of surface roughness can be identified.

Future challenges for journal bearing simulation include the precise wear prediction and the determination of wear coefficients for different bearing materials. In this context, the consideration of polymeric sliding layers in the simulation presents a new challenge for the future. While mixed lubrication can be described numerically very accurately as shown in this chapter, its escalation up to bearing failure is still beyond the scope of the presented work although relative estimations are enabled in a comparative sense based on the results. However, the numerical prediction of bearing failure requires a deeper understanding of the thermal processes in the journal bearing, which will be the subject of future work.

Acknowledgements

This work was supported by the "COMET-Competence Centers for Excellent Technologies Programme" of the Austrian Federal Ministry for Transport, Innovation and Technology (bmvit); the Austrian Federal Ministry of Science, Research and Economy (bmwfw); the Austrian Research Promotion Agency (FFG); and the Province of Styria and the Styrian Business Promotion Agency (SFG). Furthermore, we acknowledge the partial financial support provided by the Austrian Science Fund (FWF) (P27806-N30).

Author details

David E. Sander*, Hannes Allmaier and Hans-Herwig Priebsch

*Address all correspondence to: david.sander@v2c2.at

Virtual Vehicle Research Center, Graz, Austria

References

[1] Allmaier H, Offner G. Current challenges and frontiers for the EHD simulation of journal bearings: a review. SAE Technical Paper. 2016;2016-01-1856..

[2] Damm K, Pucher K, Skiadas A, Witt M. Sputter bearings for highly charged diesel engines. MTZ Worldwide. 2015;76(5):26–30.

[3] Bishop J, Nedungadi A, Ostrowski G, Surampudi B, et al. An engine start/stop system for improved fuel economy. SAE Technical Paper. 2007; 2007-01-1777. doi: 10.4271/2007-01-1777

[4] Silva C, Ross M, Farias T. Analysis and simulation of "low-cost" strategies to reduce fuel consumption and emissions in conventional gasoline light-duty vehicles. Energy Conversion and Management. 2009;50(2):215–222.

[5] Fonseca N, Casanova J, Valdés M. Influence of the stop/start system on CO2 emissions of a diesel vehicle in urban traffic. Transportation Research Part D: Transport and Environment. 2011;16(2):194–200.

[6] Mokhtar MOA, Howarth RB, Davies PB. Wear characteristics of plain hydrodynamic journal bearings during repeated starting and stopping. Tribology Transactions. 1977;20(3):191–194. doi:10.1080/05698197708982833

[7] Wilcutts M, Switkes J, Shost M, Tripathi A. Design and benefits of dynamic skip fire strategies for cylinder deactivated engines. SAE Technical Paper. 2013; 2013-01-0359. doi:10.4271/2013-01-0359

[8] Mohammadpour M, Rahmani R, Rahnejat H. The effect of cylinder de-activation on thermo-friction characteristics of the connecting rod bearing in the New European Drive Cycle (NEDC). SAE Technical Paper. 2014; 2014-01-2089.

[9] Mohammadpour M, Rahmani R, Rahnejat H. Effect of cylinder deactivation on the tribo-dynamics and acoustic emission of overlay big end bearings. Proceedings of the Institution of Mechanical Engineers, Part K: Journal of Multi-body Dynamics. 2014;228(2):138–151.

[10] Shahmohamadi H, Rahmani R, Rahnejat H, Garner CP, Dowson D. Big end bearing losses with thermal cavitation flow under cylinder deactivation. Tribology Letters. 2015;57(2):1–17. doi:10.1007/s11249-014-0444-7

[11] Holmberg K, Andersson P, Nylund NO, Mäkelä K, Erdemir A. Global energy consumption due to friction in trucks and buses. Tribology International. 2014;78:94–114.

[12] Covitch M, Brown M, May C, Selby T. Extending SAE J300 to viscosity grades below SAE 20. SAE Technical Paper. 2010; 2010-01-2286.

[13] Ligier JL, Noel B. Friction reduction and reliability for engines bearings. Lubricants. 2015;3:569–596.

[14] Macián V, Tormos B, Bermúdez V, Ramírez L. Assessment of the effect of low viscosity oils usage on a light duty diesel engine fuel consumption in stationary and transient conditions. Tribology International. 2014;79:132–139.

[15] Macián V, Tormos B, Ruiz S, Miró G. Low viscosity engine oils: study of wear effects and oil key parameters in a heavy duty engine fleet test. Tribology International. 2016;94:240–248.

[16] Allmaier H, Priestner C, Reich FM, Priebsch HH, Forstner C, Novotny-Farkas F. Predicting friction reliably and accurately in journal bearings—the importance of extensive oil-models. Tribology International. 2012;48:93–101.

[17] Knauder C, Allmaier H, Sander DE, Salhofer S, Reich FM, Sams T. Analysis of the journal bearing friction losses in a heavy-duty diesel engine. Lubricants. 2015;3:142–154.

[18] Bair S. Measurements of real non-Newtonian response for liquid lubricants under moderate pressures. Proceedings of the Institution of Mechanical Engineers, Part J: Journal of Engineering Tribology. 2001;215(3):223–233.

[19] Bair S. The shear rheology of thin compressed liquid films. Proceedings of the Institution of Mechanical Engineers, Part J: Journal of Engineering Tribology. 2002;216(1):1–17.

[20] Bair S. High pressure rheology for quantitative elastohydrodynamics. Elsevier Science, Amsterdam; 2007.

[21] Costa HL, Hutchings IM. Some innovative surface texturing techniques for tribological purposes. Proceedings of the Institution of Mechanical Engineers, Part J: Journal of Engineering Tribology. 2015;229:429–448. doi: 10.1177/1350650114539936

[22] Lu X, Khonsari MM. An experimental investigation of dimple effect on the Stribeck curve of journal bearings. Tribology Letters. 2007;27:169–176.

[23] Henry Y, Bouyer J, Fillon M. An experimental analysis of the hydrodynamic contribution of textured thrust bearings during steady-state operation: a comparison with the untextured parallel surface configuration. Proceedings of the Institution of Mechanical Engineers, Part J: Journal of Engineering Tribology. 2015;229:362–375. doi: 10.1177/1350650114537484

[24] Dadouche A, Conlon M, Dmochowski W, Koszela W, Galda L, Pawlus P. Experimental evaluation of steady-state and dynamic performance of hydrodynamic journal bearings: plain vs. textured surface. In: 10th EDF/Prime workshop; Poitiers. 2011.

[25] Dadouche A, Conlon MJ. Operational performance of textured journal bearings lubricated with a contaminated fluid. Tribology International. 2016;93:377–389.

[26] Gropper D, Wang L, Harvey TJ. Hydrodynamic lubrication of textured surfaces: a review of modeling techniques and key findings. Tribology International. 2016;94:509–529.

[27] Braun MJ, Hannon WM. Cavitation formation and modelling for fluid film bearings: a review. Proceedings of the Institution of Mechanical Engineers, Part J: Journal of Engineering Tribology. 2010;224:839–863. doi:10.1243/13506501JET772

[28] Qiu Y, Khonsari MM. Experimental investigation of tribological performance of laser textured stainless steel rings. Tribology International. 2011;44:635–644.

[29] Zhang J, Meng Y. Direct observation of cavitation phenomenon and hydrodynamic lubrication analysis of textured surfaces. Tribology Letters. 2012;46:147–158.

[30] George J, Brock R. Polymeric engine bearings for hybrid and start stop applications. SAE Technical Paper. 2012; doi:10.4271/2012-01-1966

[31] Ferreira M, Silva A, Praça M, Costa S. Polymeric coated lead free bronze bearings for high durability in medium duty diesel engines. SAE Technical Paper. 2014; doi: 10.4271/2014-36-0405

[32] Gudin D, Mian O, Sanders S. Experimental measurement and modelling of plain bearing wear in start–stop applications. Proceedings of the Institution of Mechanical Engineers, Part J: Journal of Engineering Tribology. 2013;227(5):433–446. doi: 10.1177/1350650112471287

[33] Offner G, Knaus O. A generic friction model for radial slider bearing simulation considering elastic and plastic deformation. Lubricants. 2015;3:522–538.

[34] Bobzin K, Brögelmann T. Minimizing frictional losses in crankshaft bearings of automobile powertrain by diamond-like carbon coatings under elastohydrodynamic lubrication. Surface & Coatings Technology. 2015;290:100–109.

[35] Allmaier H, Priestner C, Six C, Priebsch HH, Forstner C, Novotny-Farkas F. Predicting friction reliably and accurately in journal bearings—a systematic validation of simulation results with experimental measurements. Tribology International. 2011;44:1151–1160.

[36] Priestner C, Allmaier H, Priebsch HH, Forstner C. Refined simulation of friction power loss in crank shaft slider bearings considering wear in the mixed lubrication regime. Tribology International. 2012;46(1):200–207. 10.1016/j.triboint.2011.03.012

[37] Patir N, Cheng H. An average flow model for determining effects of three-dimensional roughness on partial hydrodynamic lubrication. ASME Journal of Lubrication Technology. 1978;100:12–17.

[38] Patir N, Cheng H. Application of average flow model to lubrication between rough sliding surfaces. ASME Journal of Lubrication Technology. 1979;101(2):220–229.

[39] Jakobsson B, Floberg L. The finite journal bearing, considering vaporization. Gumperts Förlag. 1957.

[40] Krasser J. Thermoelastohydrodynamische Analyse dynamisch belasteter Radialgleitlager [dissertation]. Graz University of Technology; 1996.

[41] Greenwood J, Tripp J. The contact of two nominally flat rough surfaces. Proceedings of the Institution of Mechanical Engineers. 1970;185(1):625–633.

[42] Sander DE, Allmaier H, Priebsch HH, Reich FM, Witt M, Skiadas A, Knaus O. Edge loading and running-in wear in dynamically loaded journal bearings. Tribology International. 2015;92:395–403.

[43] Sander DE, Allmaier H, Priebsch HH, Witt M, Skiadas A. Simulation of journal bearing friction in severe mixed lubrication – validation and effect of surface smoothing due to running-in. Tribology International. 2016;96:173–183.

[44] Vogel H. The law of the relation between the viscosity of liquids and the temperature. Physikalische Zeitschrift. 1921;22:645-646.

[45] Barus C. Isothermals, isopiestics and isometrics relative to viscosity. American Journal of Science. 1893;266:87-96.

[46] Cross MM. Rheology of non-Newtonian fluids: a new flow equation for pseudoplastic systems. Journal of Colloid Science. 1965;20(5):417–437.

[47] Sander DE, Allmaier H, Priebsch HH, Reich FM, Witt M, Füllenbach T, Skiadas A, Brouwer L, Schwarze H. Impact of high pressure and shear thinning on journal bearing friction. Tribology International. 2015;81:29–37.

[48] Allmaier H, Sander DE, Priebsch HH, Witt M, Füllenbach T, Skiadas A. Non-Newtonian and running-in wear effects in journal bearings operating under mixed lubrication. Proceedings of the Institution of Mechanical Engineers, Part J: Journal of Engineering Tribology. 2015;230(2):135–142.

[49] Damm K, Skiadas A, Witt M, Schwarze H. Gleitlagererprobung Anhand der Forderungen des Automobilmarkts. ATZextra. 2010;15(1):54–63.

[50] Offner G. Friction power loss simulation of internal combustion engines considering mixed lubricated radial slider, axial slider and piston to liner contacts. Tribology Transactions. 2013;56(3):503–515.

[51] Allmaier H, Priestner C, Reich FM, Priebsch HH , Novotny-Farkas F. Predicting friction reliably and accurately in journal bearings-extending the simulation model to TEHD. Tribology International. 2013;58:20–28.

[52] Allmaier H, Priestner C, Sander DE, Reich F. Friction in automotive engines. In: H Pihtili, editor. Tribology in engineering. Intech; 2013. p. 149–184. http://dx.doi.org/10.5772/51568

[53] Sander DE. A validated elasto-hydrodynamic simulation for journal bearings operating in severe conditions [unpublished doctoral dissertation]. Graz, Austria: Graz University of Technology; 2016.

[54] Blau PJ. On the nature of running-in. Tribology International. 2006;38(11):1007–1012.

[55] Archard J. Contact and rubbing of flat surfaces. Journal of Applied Physics. 1953;24(8): 981–988.

[56] Morina A, Neville A. Understanding the composition and low friction tribofilm formation/removal in boundary lubrication. Tribology International. 2007;40:1696–1704.

[57] Bouyer J, Fillon M. Experimental measurement of the friction torque on hydrodynamic plain journal bearings during start-up. Tribology International. 2011;44:772–781.